Northumbria Research Link

Citation: Zheng, Mingming, Ren, Jiajia, Wang, Chuanjin, Ma, Yong, Ding, Jianxu, Li, Tingxi, Elnaggar, Ashraf, El Azab, Islam, Mahmoud, M.H.H., El-Bahy, Salah, Seok, IIwoo, Naik, Nithesh, Roymahapatra, Gourisankar, Murugadoss, Vignesh, Huang, Mina, Xu, Bin and Guo, Zhanhu (2022) Magnetite@poly(p-phenylenediamine) core-shell composite modified with salicylaldehyde for adsorption and separation of Mn (VII) from polluted water. Journal of Nanostructure in Chemistry, 12 (6). pp. 1155-1168. ISSN 2193-8865

Published by: Springer

URL: https://doi.org/10.1007/s40097-022-00510-4 <https://doi.org/10.1007/s40097-022-00510-4>

This version was downloaded from Northumbria Research Link: https://nrl.northumbria.ac.uk/id/eprint/49767/

Northumbria University has developed Northumbria Research Link (NRL) to enable users to access the University's research output. Copyright © and moral rights for items on NRL are retained by the individual author(s) and/or other copyright owners. Single copies of full items can be reproduced, displayed or performed, and given to third parties in any format or medium for personal research or study, educational, or not-for-profit purposes without prior permission or charge, provided the authors, title and full bibliographic details are given, as well as a hyperlink and/or URL to the original metadata page. The content must not be changed in any way. Full items must not be sold commercially in any format or medium without formal permission of the copyright holder. The full policy is available online: http://nrl.northumbria.ac.uk/policies.html

This document may differ from the final, published version of the research and has been made available online in accordance with publisher policies. To read and/or cite from the published version of the research, please visit the publisher's website (a subscription may be required.)

Northumbria University NEWCASTLE

UniversityLibrary

Magnetite@poly(p-phenylenediamine) core-shell composite modified with salicylaldehyde for adsorption and separation of Mn (VII) from polluted water

Mingming Zheng‡[1], Jiajia Ren‡[1], Chuanjin Wang[1], Yong Ma[1,*], Jianxu Ding[1], Tingxi Li[1,*], Ashraf Y. Elnaggar[2], Islam H. El Azab[2], M.H.H. Mahmoud[3], Salah M. El-Bahy[4], IIwoo Seok[5], Nithesh Naik[6], Gourisankar Roymahapatra[7], Vignesh Murugadoss[8], Mina Huang[8], Ben Bin Xu,[9] Zhanhu Guo[8,*]

[1]School of Material Science and Engineering, Shandong University of Science and Technology, Qingdao 266590, P. R. China

[2] Department of Food Science and Nutrition, College of Science, Taif University, P.O. box 11099, Taif 21944, Saudi Arabia

[3]Department of Chemistry, College of Science, Taif University, P.O. Box 11099, Taif 21944, Saudi Arabia.

[4]Department of Chemistry, Turabah University College, Taif University, P.O.Box 11099, Taif 21944, Saudi Arabia

[5] Mechanical Engineering, Arkansas State University, Jonesboro, Arkansas, 72401, USA

[6] Department of Mechanical & Manufacturing Engineering, Manipal Institute of Technology, Manipal Academy of Higher Education, Manipal-576104, Karnataka, India

[7] School of Applied Science and Humanities, Haldia Institute of Technology, Haldia 721657, India

[8] Integrated Composites Laboratory (ICL), Department of Chemical and Biomolecular Engineering, University of Tennessee, Knoxville, TN, 37996, USA

[9] Mechanical and Construction Engineering, Faculty of Engineering and Environment, Northumbria University, Newcastle upon Tyne NE1 8ST, UK

‡Equal contribution first author

* Correspondence author: courage2010@126.com (Y. Ma); litx@sdust.edu.cn (T. Li); zguo10@utk.edu (Z. Guo).

Abstract

Magnetite@poly-p-phenylenediamine (Fe_3O_4@PpPD) composite modified with salicylaldehyde (SA) was fabricated as adsorbent to remove Mn (VII) from wastewater. The Fe_3O_4 microspheres endow the adsorbent with the ability of rapid solid-liquid separation. The PpPD with acid and alkali resistance can protect Fe_3O_4 from corrosion while introducing a large amount of N atoms to adsorb Mn (VII). The introduction of SA increases the specific surface area and adsorption sites of the adsorbent. The effects of pH, time and temperature on the adsorption process were studied. At pH=2, the maximum adsorption capacity (Q) is as high as 148.34 mg g^{-1}, which is attributed to the complexation/chelation and electrostatic interaction between amino and hydroxyl groups and Mn (VII). It is found that the adsorption process conforms to the pseudo-second order kinetic model and Langmuir isotherm model. Thermodynamics researches demonstrate that the adsorption is a spontaneous endothermic process. After four adsorption cycle tests, the adsorption capacity losses only 1%. Moreover, high adsorption efficiency in river water and mixed metal ions solution proves that the prepared Fe_3O_4@PpPD-SA composite possesses excellent Q in removing Mn (VII).

Keywords: Magnetic adsorbent; Fe_3O_4 microspheres; Poly-p-phenylenediamine; Salicylaldehyde; Mn (VII).

1. Introduction

In recent years, many industrial processes discharge a large amount of wastewater which contains organic and inorganic pollutants, posing a serious health hazard to organisms [1]. Non-biodegradable manganese ion pollutants mainly stem from the mining and smelting of manganese-containing ore and the production process of manganese alloys[2]. As an essential trace element for the human body, lack of manganese intake can cause manganese deficiency symptoms, for example wounds difficult to heal. However, excessive intake of this element can also cause chronic poisoning and severely damage the human nervous system. Therefore, how to remove manganese in wastewater to meet the requirements of discharge (the content of manganese is not more than 2 mg L^{-1}) is an urgent problem to be solved[3-5].

So far, many technologies have been applied to remove and recover toxic metal ions in sewage, for instance precipitation, electrolysis, reverse osmosis, membrane filtration and adsorption, etc[6-9]. The adsorption technology is widely used because of its simple design, easy operation and wide selection range[10-12]. In order to further reduce the cost and simplify the operation, the synthesis and the modification of adsorbents are usually carried out by compounding organic substances on magnetic inorganic bodies to realize the rapid separation of adsorbents. With the advance of advanced materials and energy devices, conductive polymers are gradually coming into the public eye[13-21]. Due to the ease of synthesis, controllable structure, good acid and alkali resistance, and a large number of adsorbed functional groups, conductive polymers have gradually increased in the trend of introducing polymers as adsorbents in water treatment[22-24]. Poly-p-phenylene diamine (PpPD) is not only chemically stable and easy to prepare[25-29], but also has a large number of nitrogen-containing groups, making it widely used to remove heavy metal ions in water[30-34]. For instance, Munzhelele et al. synthesized iron-doped PpPD composite materials to remove toxic metal ions As^{3+} in water[35]. Mdlalose et al. used synthetic PpPD to reduce Cr (VI) in solution to Cr (III)[30]. Min et al. studied the influence of PpPD microstructure on the adsorption capacity of

removing lead ions[36].

Both the hydroxyl group and the aldehyde group in salicylaldehyde (SA) contain oxygen atoms which can bind to the metal ions in the solution through coordination[37-42]. SA is usually used for the modification of composite materials to improve the adsorbents performance. Zhang et al. used double SA Schiff base (SBA-DSA) to modify SBA-15 mesoporous silica to adsorb and separate Cu (II) and Pb (II) ions from the aqueous solution[43]. Hussain et al. prepared SA-functionalized chitosan nanoparticles as adsorbents for Cu (II), Cd (II) and Pb (II) ions[37]. Therefore, it can be assumed that the Fe_3O_4@PpPD core-shell composite modified with SA can significantly enhance the adsorption property and actualize the adsorption for Mn (VII).

In this study, Fe_3O_4@PpPD-SA composite was synthesized by hydrothermal method, chemical oxidation polymerization method and chemical modification method in turn. The PpPD with the acid and alkali resistance can protect Fe_3O_4 from corrosion, and introduces a large amount of N atoms to adsorb Mn (VII) in the solution. Moreover, the introduction of SA increases the specific surface area and adsorption sites of the adsorbent for Mn (VII). Fe_3O_4@PpPD-SA composite combines the adsorption characteristics of PpPD and SA and plays the characteristics of double adsorption, greatly improving the Mn (VII) adsorption efficiency. The influence of time, pH and temperature on Mn (VII) adsorption efficiency were researched under different experimental conditions. In addition, the adsorbent can be quickly separated from the solution with the help of an external magnetic field, which has an excellent development prospect in removing heavy metal ions in wastewater.

2 Experiment

2.1 Materials

Ferric chloride ($FeCl_3 \cdot 6H_2O$, 99%), sodium citrate ($Na_3C_6H_5O_7 \cdot 2H_2O$, 99%), urea ($CH_4N_2O$, 99%), sodium polyacrylate ($(C_3H_3NaO_2)_n$), p-phenylenediamine ($C_6H_8N_2$, 99%), ammonium persulfate ($(NH_4)_2S_2O_8$, APS, 98%), salicylaldehyde ($C_7H_6O_2$, SA, 99%), ethanol (CH_3CH_2OH),

ammonia ($NH_3 \cdot H_2O$, 25%-28%), silane coupling agent KH-550 (98%) and potassium permanganate ($KMnO_4$).

2.2 Fabrication of Fe_3O_4@PpPD-SA

2.2.1 Synthesis of Fe_3O_4 microspheres

0.7 g $FeCl_3 \cdot 6H_2O$, 1.5 g $Na_3C_6H_5O_7 \cdot 2H_2O$ and 0.5 g CH_4N_2O were sequentially added to 20 mL deionized water, followed by fully stirring to obtain a homogeneous solution. Then add the resulting solution dropwise to 20 mL $(C_3H_3NaO_2)_n$ solution. Finally, the mixed solution was transferred to a 50 mL stainless steel reactor lined with polytetrafluoroethylene and reacted at 200 °C for 20 h. Applying a magnet to magnetically separate the sediment, and wash completely. The precipitate was dried in an oven at 60 °C for 12 h to obtain Fe_3O_4.

2.2.2 Synthesis of Fe_3O_4@PpPD

0.5 g Fe_3O_4 was ultrasonically dispersed in 150 mL absolute ethanol and 50 mL deionized water for 30 min and added to a round bottom flask, and then 5 mL $NH_3 \cdot H_2O$ and 20 mL KH-550 were also added. The reactor was placed in a 70 °C constant temperature water bath and stirred for 24 h. Add 0.27 g of p-PD and 1.141 g of APS to 50 mL of distilled water, add them to the round bottom flask and stir for 12 h. The sample was magnetically separated, washed with absolute ethanol and deionized water, and placed in an oven at 60 °C for 12 h to obtain Fe_3O_4@PpPD composite material.

2.2.3 Synthesis of Fe_3O_4@PpPD-SA

0.5 g Fe_3O_4@PpPD composite was totally dispersed in 180 mL absolute ethanol and added to a round bottom flask, and then 25 mL SA was also added. Place the reactor in a 70 °C constant temperature water bath and stir for 8 h. After the reaction, the sample was magnetically separated and washed with absolute ethanol, and placed in an oven at 60 °C to dry for 12 h to obtain Fe_3O_4@PpPD-SA composite material.

2.3 Characterizations

Characterize the morphology of composite materials by scanning electron microscope (SEM, Apreo S HiVac) and transmission electron microscope (TEM, JEOL JEM-3010). X-ray diffractometer (XRD, Rigaku Utima IV) was used for phase analysis of the test material. Fourier transform infrared spectroscopy (FTIR, Nicolet iS50) detects the chemical groups of materials. X-ray photoelectron energy spectrum analyzer was used to analyze the valence state of elements (XPS, ESCALAB XI+). The hysteresis loops of the experimental samples were measured using a Lakeshore-7307 vibrating sample magnetometer (VSM, LakeShore 7404). The specific surface area of the experimental sample was determined by an automatic specific surface and porosity analyzer (BET, Mack ASAP 2460). The concentration changes of Mn (VII) was detected with an ultraviolet-visible spectrophotometer (UV-vis, 5200PC).

2.4 Adsorption process

2.4.1 The effect of pH on adsorption capacity

A 500 mL volumetric flask was used to prepare 150 mg L^{-1} $KMnO_4$ solution. And 50 mL $KMnO_4$ solution and 50 mg adsorbent were placed in different colorless transparent plastic beakers, and the pH was adjusted to 2-11 by using HCl and NaOH solution. After 6 h of adsorption at 20 °C, 3 mL of supernatant was taken for determination. The adsorption capacity of the adsorbent for Mn (VII) is confirmed by change in the absorbance of the test solution at a wavelength of 525 nm. The calculation formula[44] is as Eq. (1):

$$Q=\frac{(C_0-C_t)V}{m} \quad (1)$$

In here, Q represents adsorption capacity (mg g^{-1}); C_0 represents the initial concentration of the solution (mg L^{-1}), and C_t represents the concentration of the solution at moment t; V represents the volume of $KMnO_4$ solution (L); m represents the mass of Fe_3O_4@PpPD-SA composite (g).

2.4.2 Adsorption kinetics test

50 mL $KMnO_4$ solution with a concentration of 150 mg L^{-1} and 50 mg adsorbent were put into a beaker, and the solution was adjusted to pH=2 through using HCl solution. The adsorption lasted

6 h at 25 °C. Take out 3 mL supernatant every 30 min, and measure the adsorption efficiency of the adsorbent for Mn (VII) at the wavelength of 525 nm. The calculation formula[45] is as Eq. (2):

$$q=\frac{C_0-C_e}{C_0}\times 100 \quad (2)$$

In here, q represents adsorption efficiency; C_e represents equilibrium concentration of Mn (VII) (mg L^{-1}).

2.4.3 Adsorption thermodynamic test

50 mL $KMnO_4$ solution with a concentration of 150 mg L^{-1} and 50 mg adsorbent were placed in different colorless transparent plastic beakers, adjusted to pH=2, and then placed at 20, 30 and 40 °C water bath. After 5 h adsorption, 3 mL supernatant was applied to obtain the Q of Mn (VII) by measuring the degree of change in the absorbance of the solution at a wavelength of 525 nm. The calculation formula is as shown in formula (1).

2.4.4 Adsorption cycle test

The adsorbed Fe_3O_4@PpPD-SA was fully reacted in 0.1 M H_2SO_4 for 48 h. After the reaction, a magnetic field was applied to magnetically separate the reacted mixed solution, and washed several times with ethanol and deionized water until the upper layer was clear and transparent. The lower precipitate was placed in a 60 °C oven for 24 h to obtain Fe_3O_4@PpPD-SA to proceed to the next adsorption-desorption cycle.

3.4.5 Selective adsorption test

Take a certain amount of river water and filter it sufficiently to obtain a clear liquid. 100 mg L^{-1} $KMnO_4$ solutions were prepared with river water, tap water and distilled water as solvents, respectively. The river water was taken from the man-made river named Moshui River in the university. The tap water is taken from the tap. The monitoring of water quality demonstrated that the ion concentration in both tap water and river water was much lower than the target ion concentration. 50 mL $KMnO_4$ solution and 20 mg sorbent were placed in a 150 mL colorless transparent plastic cup, and the pH was adjusted to 2 with HCl. The adsorption temperature was at

25 °C. After the adsorption, 3 mL magnetically separated supernatant was taken for testing. The adsorption efficiency of Mn (VII) was determined by measuring the degree of change in the absorbance of the solution (at a wavelength of 525 nm) with a UV-vis spectrophotometer.

50 mL, 100 mg L^{-1} $AlCl_3$, NaCl and $ZnCl_2$ solutions were successively placed in a 150 mL colorless transparent plastic cup, and then 0.29 g $KMnO_4$ and 20 mg Fe_3O_4@PpPD-SA were added. It was used with distilled water as solvent to prepare 100 mg L^{-1} $KMnO_4$ solution for adsorption in the same environment. After the adsorption, 3 mL magnetically separated supernatant was taken for testing. The adsorption efficiency of Mn (VII) was determined by measuring the degree of change in the absorbance of the solution (at a wavelength of 525 nm) with a UV-vis spectrophotometer.

3. Results and discussion

3.1 Synthesis and characterization of Fe_3O_4@PpPD-SA composites

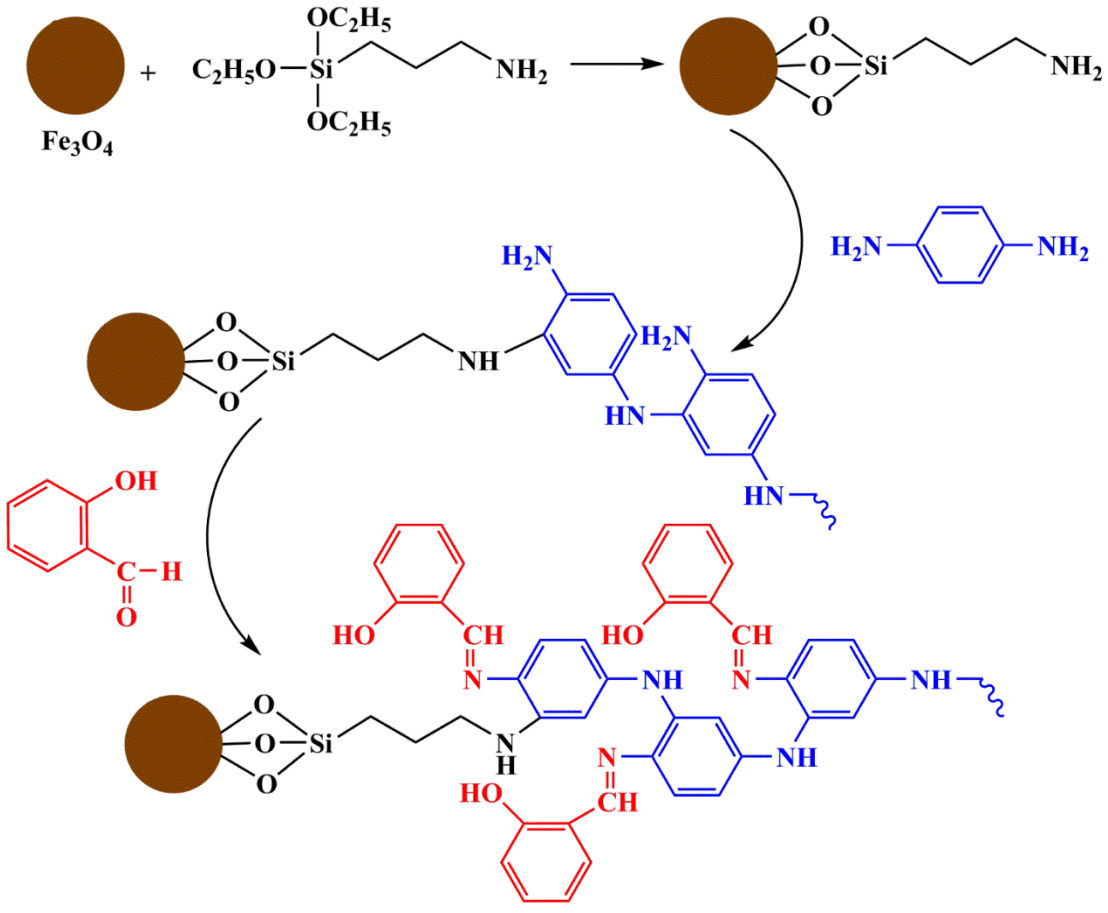

Figure 1 The preparation process of Fe_3O_4@PpPD-SA composite.

Figure 1 illustrates the preparation process of Fe_3O_4@PpPD-SA composite. Firstly, magnetic Fe_3O_4 microspheres are fabrication via a hydrothermal method. It can be seen from SEM image of Figure 2 (a) that these Fe_3O_4 microspheres with an average diameter of about 258.75 nm have rough and uneven surfaces, which greatly enhance the contact area with the solution. This case is beneficial to the subsequent coating process. Then, utilizing the bridge function of silane coupling agent between inorganic and organic parts, as well as APS serving as oxidant, the periphery of Fe_3O_4 microspheres are successfully coated with a layer of PpPD. From SEM image of Figure 2 (b), one can clearly view that the PpPD completely coats on the surface of Fe_3O_4 microspheres to form core@shell structure. Meanwhile, their diameter increase to about 317.07 nm, also demonstrating the successful preparation of the PpPD coating shell and its thickness estimated to be 29.16 nm. Finally, SA is used to functionally modify Fe_3O_4@PpPD composite. The aldehyde group of SA is connected to the amino group of the PpPD, and a large number of O atoms are successfully introduced, thus improving the adsorption performance. In SEM image of Figure 2 (c), the morphology of Fe_3O_4@PpPD-SA composite has almost no change compared with the former composite except for the slightly increased diameter. This situation indicates that the modification of SA has little effect on the morphology of the resulting composite. In addition, the TEM images of Fe_3O_4 microspheres, Fe_3O_4@PpPD composite and Fe_3O_4@PpPD-SA composite can also be observed, as shown in Figure 2(d)(e)(f), in agreement with the outcomes of their SEM images.

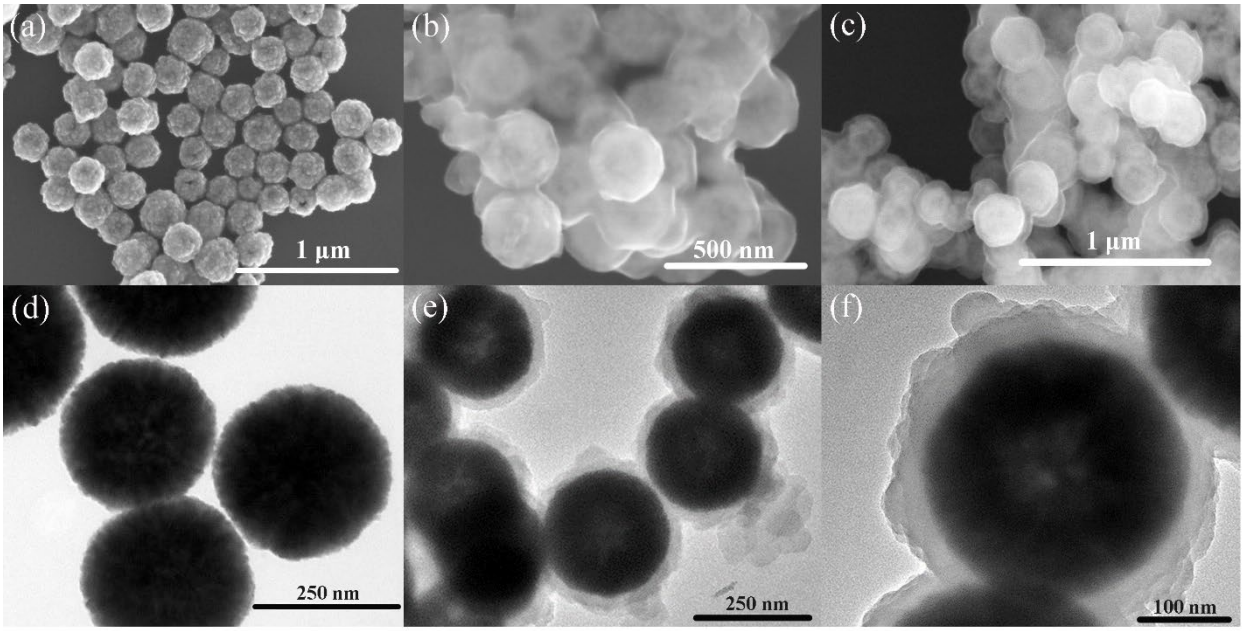

Figure 2 SEM images of Fe_3O_4 microspheres (a), Fe_3O_4@PpPD composite (b), Fe_3O_4@PpPD-SA composite (c), and their corresponding TEM images (d) (e) (f).

Figure 3 (a) (b) shows the XRD and FTIR spectra of Fe_3O_4 (I), Fe_3O_4@PpPD (II) and Fe_3O_4@PpPD-SA composite (III). With regard to XRD patterns, the first sample exhibits sharp diffraction peaks at 2θ=30.07°, 35.44°, 43.09°, 53.43°, 57.13°, 62.62° and 74.11°, which correspond to (220), (311), (400), (422), (511), (440) and (533) (JCPDS Card No. 88-0315) structural phases[46], indicating the synthesized Fe_3O_4 microspheres having good crystallinity. The last two display a new large and broad diffraction peak at 2θ=15-25°, manifesting that the prepared PpPD coating shell and the modified SA possess an amorphous structure. In the meantime, it is noteworthy that the characteristic peaks of Fe_3O_4 still exists, but they are significantly weakened. This case suggests the blocking effect of the formed polymers, further demonstrating the successful preparation of Fe_3O_4@PpPD and Fe_3O_4@PpPD-SA composite.

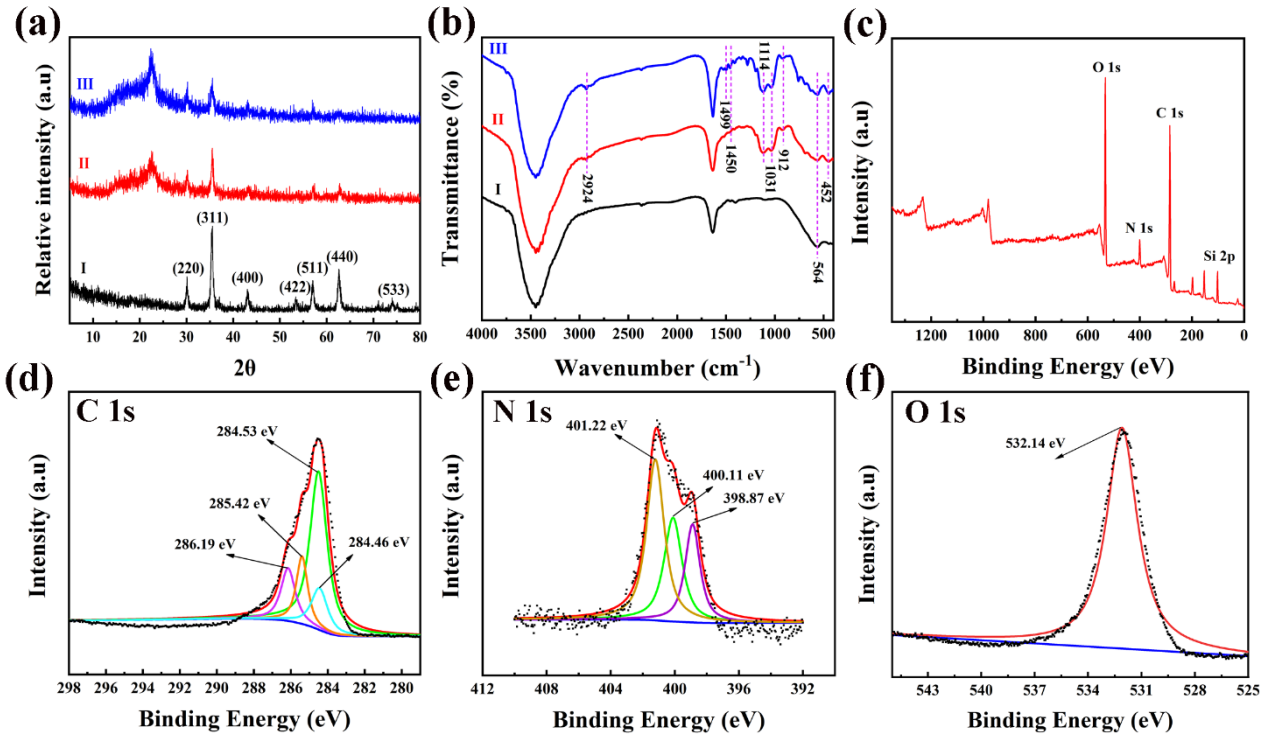

Figure 3 XRD patterns (a) and FTIR spectra (b) of Fe_3O_4 microspheres (I), Fe_3O_4@PpPD composite (II) and Fe_3O_4@PpPD-SA composite (III); XPS spectra of Fe_3O_4@PpPD-AP composite (c), C 1s (d), N 1s (e) and O 1s (f).

As for FTIR spectra, the strong peak at 564 cm^{-1} of all samples corresponds to the Fe-O vibration stemming from Fe_3O_4 microspheres[47, 48]. The peak at 452 cm^{-1} for the last two composites is attributed to the Si-O vibration of silane coupling agent, which plays a role in linking Fe_3O_4 microspheres and PpPD coating shell. The typical C-H stretching vibration occurs at 912 cm^{-1} [49]. The signal at 1031 cm^{-1} is associated with the aromatic C-H in the plane bending mode. The peak positions at 1407 cm^{-1} and 1450 cm^{-1} represent the benzene ring. The broad band near 2924 cm^{-1} represents the N-H stretching vibration[50]. The above peaks powerfully prove the formation of PpPD. For Fe_3O_4@PpPD-SA, the new peak at 1499 cm^{-1} represents C=N stretching vibration[51], which signifies the successful modification of SA on the surface of Fe_3O_4@PpPD composite.

From Figure 3 (c), it can be found that the XPS spectrum of Fe_3O_4@PpPD-SA composite has four peaks at 531.57 eV, 401.06 eV, 283.48 eV and 100.65 eV, separately corresponding to O 1s, N 1s, C 1s and Si 2p [52]. The C 1s spectrum described in Figure 3 (d) has four peaks at 284.46 eV,

284.53 eV, 285.42 eV and 286.19 eV, successively ascribed to C-N, C-C, C-O and C=N [53]. The three high-resolution peaks in the N 1s spectrum in Figure 3 (e) appear at 401.04 eV, 400.38 eV and 399.54 eV correspond to -NH- connected with p-PD, -NH_2 of p-PD and -N= connected with SA, respectively. The O 1s spectrum displayed in Figure 3 (f) has only one Si-O peak at 532.14 eV, which proves that the Fe_3O_4 microspheres are completely covered, in line with the result of TEM image.

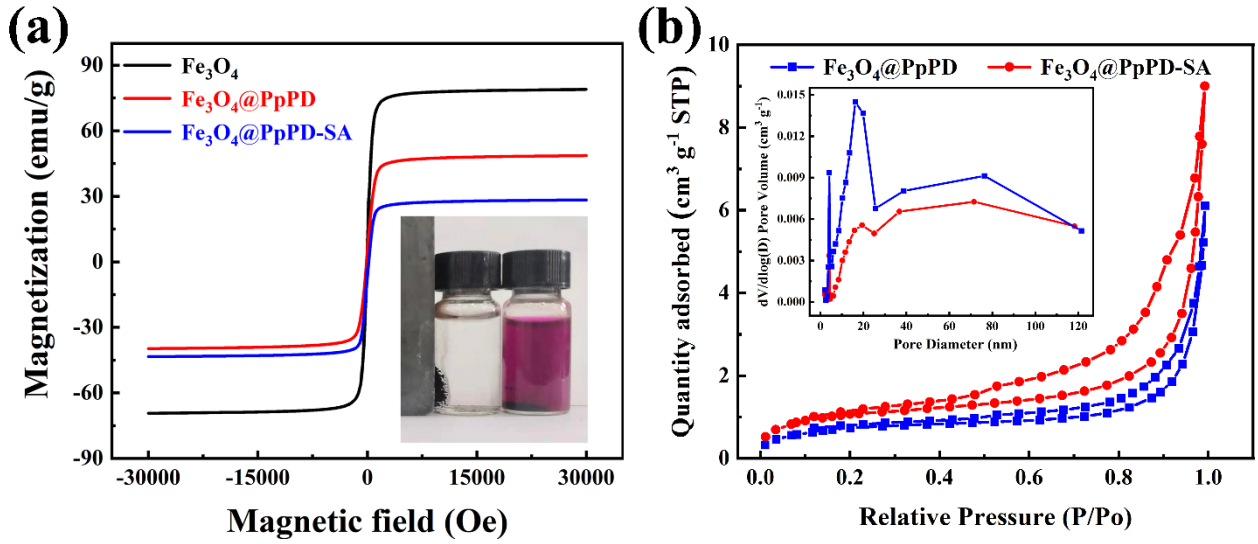

Figure 4 (a) Hysteresis loops of Fe_3O_4 microspheres, Fe_3O_4@PpPD composite, Fe_3O_4@PpPD-SA composite measured at room temperature; inset image of the solution comparison before and after adsorption and the magnetic separation effect, (b) N_2 adsorption-desorption isotherms of Fe_3O_4@PpPD composite and Fe_3O_4@PpPD-SA composite.

The magnetic properties of the adsorbent were studied as shown in Figure 4 (a). The zero coercivity and reversible hysteresis behavior indicate that the adsorbent has superparamagnetic nature[54, 55]. The saturation magnetization values of Fe_3O_4 nanoparticles, Fe_3O_4@PpPD and Fe_3O_4@PpPD-SA composites are 78.84, 48.58 and 28.32emu g^{-1}, respectively. Although the magnetic properties gradually decrease with the increase of the organic shell, the finally synthesized adsorbent Fe_3O_4@PpPD-SA composite still has good magnetic properties and can achieve rapid solid-liquid separation after the adsorption is completed, as shown in inset image. Figure 4 (b) shows the BET surface area of Fe_3O_4@PpPD and Fe_3O_4@PpPD-SA composite. Compared with the former 2.56 m^2 g^{-1}, the latter value increases to 3.69 m^2 g^{-1}, and the BJH desorption cumulative volume

increases from 0.008 cm^3 g^{-1} to 0.013 cm^3 g^{-1}. In addition, the BJH desorption average pore diameter of Fe_3O_4@PpPD-SA composite is 24.45 nm, which is significantly larger than that of Fe_3O_4@PpPD composite. The results show that the modification of Fe_3O_4@PpPD with SA not only introduces more adsorption functional groups, but also increases the contact area between the adsorbent and the adsorbate[56], which greatly improves the adsorption performance.

3.2 The adsorption performance of Fe_3O_4@PpPD-SA composite for Mn (VII)

3.2.1 Research on the influencing factors of adsorption

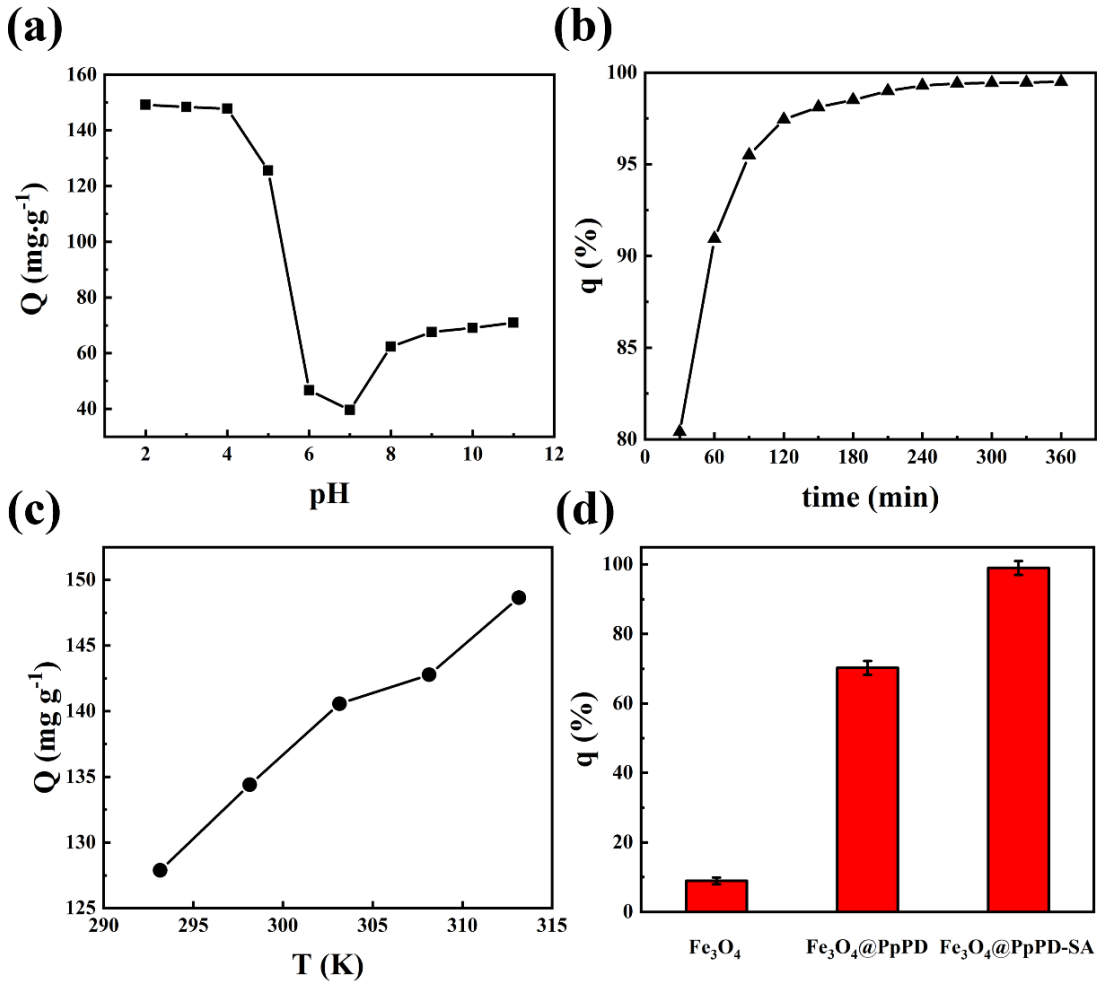

Figure 5 The influences of pH (a), time (b), temperature (c) and adsorbent type (d) on the adsorption.

The factors affecting the adsorption of Fe_3O_4@PpPD-SA composite material were investigated, as shown in Figure 5. Figure 5(a) clearly shows that the adsorption performance is the best under

acidic conditions, followed by alkaline conditions, and the worst under neutral conditions. Under acidic conditions, the Q increases with the decrease of pH, and at pH=2 reaches the best value of 148.34 mg g^{-1}. Under alkaline conditions, the q increases with the increase of pH. The reason for these phenomena is closely ascribed to the functional groups contained in composite.

Figure 6 displays that the adsorption mechanism of Fe_3O_4@PpPD-SA composite to Mn (VII) mainly depends on the functional groups containing N and O. When the pH is much lower than pH_0 (the pH value of adsorbent surface with zero charge), N-containing group will be protonated ($-NH_x^+$). For the free MnO_4^- in the form of anions, NH_x^+ will have electrostatic attraction with them to achieve the adsorption. In the case of $pH>pH_0$, N-containing group will form negative ions ($-NH_xOH^-$), and the electrostatic effect inhibits their adsorption of MnO_4^-[57]. Therefore, the q under alkaline conditions is significantly lower than those under acidic conditions. In addition, the phenolic hydroxyl group can easily react with MnO_4^- under acidic conditions, and alkaline conditions can inhibit this reaction to a certain extent[58]. In general, Fe_3O_4@PpPD-SA composite has the best adsorption effect on Mn (VII) under acidic conditions.

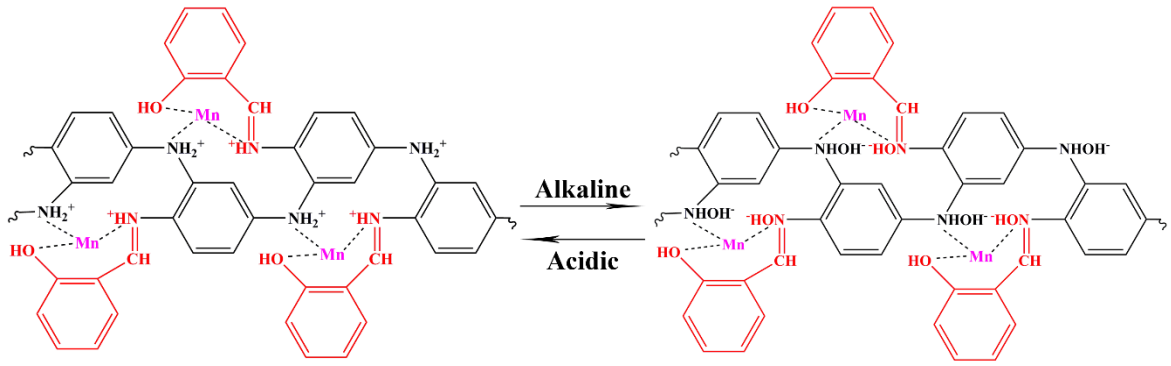

Figure 6 Adsorption mechanism of Fe_3O_4@PpPD-SA for Mn (VII).

With the increase of time, Figure 5 (b) presents the increased q, especially in the first 60 min of adsorption, and the value can reach to 90.95%. This is mainly due to the high initial adsorption concentration of Mn (VII) and abundant adsorption binding sites of the adsorbent. As time increases, the solution concentration decreases and the binding sites become saturated, leading to the adsorption rate gradually decreases. Finally, the adsorption equilibrium is reached at about 360 min,

at which time the q is as high as 99.58%. Under the same conditions, the relationship between Q and temperature is displayed in Figure 5 (c). The higher the temperature is, the greater the adsorbed amount of Mn (VII) is. The Q is 148.65 mg g^{-1} at 40 °C, far exceeding 20.70 mg g^{-1} at 20 °C, indicating that the high temperature favors the adsorption process. This case is a result of the enhanced movement of Mn (VII) and the adsorbent under high temperature, increasing collision probability with each other.

The q comparison chart of Fe_3O_4 microspheres, Fe_3O_4@PpPD composite and Fe_3O_4@PpPD-SA composite can be observed in Figure 5 (d). There is no doubt that the q of the first sample is very poor, and its value is only 8.93%. The reason is that only physical adsorption occurs between Fe_3O_4 microspheres and Mn (VII) during the adsorption process. Coating PpPD on the surface of Fe_3O_4 microspheres greatly improves the q to 70.26%, which is attributed to the adsorption of PpPD coating shell. For the last, the q is 98.99%, mainly owing to the double adsorption of PpPD and SA. Hence, the elaborately prepared Fe_3O_4@PpPD-SA composite possesses extremely excellent adsorption performance.

3.2.2 Adsorption kinetics

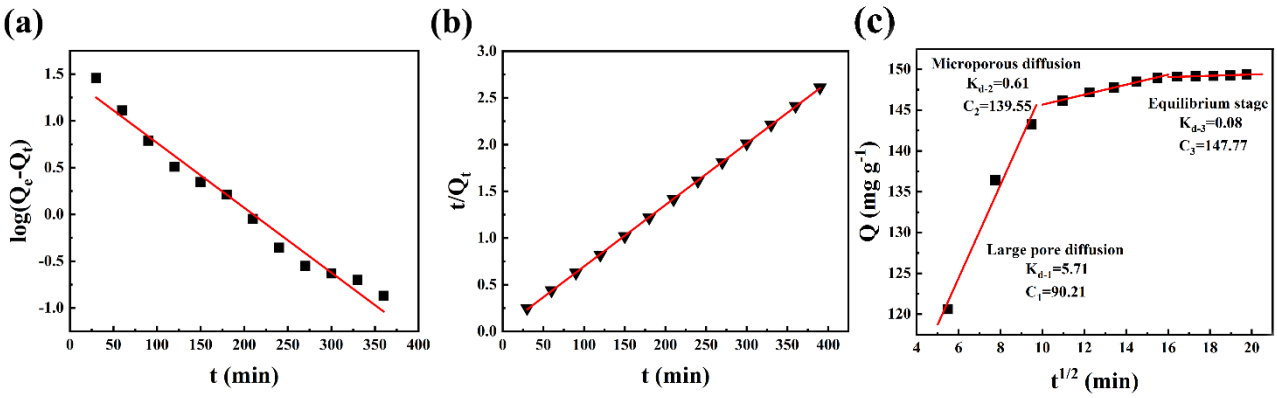

Figure 7 Pseudo first-order model (a), pseudo second-order model (b) and intra-particle diffusion model (c) of Fe_3O_4@PpPD-SA adsorption of Mn (VII).

The rate equations expressed by pseudo first-order model (Eq. (3)) and pseudo second-order model (Eq. (4))[59] proposed by Lagergren are used to analyze the rate kinetics of Mn (VII) adsorption by Fe_3O_4@PpPD-SA composites:

$$\log (Q_e - Q_t) = \log Q_e - \frac{k_1 t}{2.303} \quad (3)$$

$$\frac{t}{Q_t} = \frac{t}{Q_e} + \frac{1}{h_0} \quad (4)$$

In here, Q_e and Q_t are Mn (VII) adsorbed on Fe_3O_4@PpPD-SA composite at equilibrium and moment t, respectively (mg g^{-1}); k_1 represents the rate constant of pseudo first-order adsorption (min^{-1}); h_0 represents the initial adsorption (min g mg^{-1}).

Figure 7 exhibits the fitting curves of pseudo first-order model (a) and pseudo second-order model (b), respectively. It can be seen intuitively that the adsorption of Mn (VII) is more suitable to be explained by pseudo second-order model. Moreover, the kinetic model is usually selected through comparing the degree of approximation between R^2 and 1[60]. Table 1 shows all kinetic parameters of these two models. Of particular importance is that R^2=0.99 of pseudo second-order model is prominently higher than R^2=0.97 of pseudo first-order model. Therefore, pseudo second-order model herein is chosen to explain adsorption kinetics.

Table 1 Kinetic parameters of Fe_3O_4@PpPD-SA composite for Mn (VII) adsorption under pH=2 at 25 °C.

	K_1 (min^{-1})	Q_e (mg g^{-1})	K_2 (g mg^{-1} min^{-1})	h_0 (min g mg^{-1})	R^2
Pseudo-first order model	0.02	28.76	--	--	0.97
Pseudo-second order model	--	151.98	1.31	25.99	0.99

In addition, intra-particle diffusion model of Eq. (5)[61] is used to study whether the diffusion process between particles or other diffusion processes controls the speed of the reaction during the adsorption process:

$$Q_t = K_{d\text{-}i} t_{\frac{1}{2}} + C_i \quad (5)$$

In here, $K_{d\text{-}i}$ is the rate constant (min^{-1}); C_i is the thickness of the boundary layer (mg g^{-1}); i is the number of diffusion stages.

It can be seen from Figure 7 (c) that the whole process of Mn (VII) adsorption by Fe_3O_4@PpPD-SA can be divided into four stages: (1) Boundary layer diffusion. The concentration difference of the ions drives the aggregation of dye ions from the solution phase to the adsorbent surface (infinitely close to the surface); (2) Large pore diffusion. This stage has the fastest adsorption speed, with the largest rate constant $K_{d\text{-}1}$ and the smallest boundary layer thickness C_1; (3) Microporous diffusion. This stage corresponds to the medium adsorption rate constant $K_{d\text{-}2}$ and boundary layer thickness C_2; (4) Equilibrium stage. This stage corresponds to the minimum rate constant $K_{d\text{-}3}$ and the maximum boundary layer thickness C_3.

By comparing the rate constants $K_{d\text{-}i}$ and the boundary layer thickness C_i at each stage, it can be found that the intraparticle diffusion rate gradually decreases as the reaction proceeds. It shows that the third stage (micropore diffusion) and the fourth stage (equilibrium stage) are the main steps for controlling the adsorption[53].

3.2.3 Isotherm models

Langmuir and Freundlich isotherm models are applied to analyze isotherm data. The former characterizing the monolayer adsorption process[62] is represented by Eq. (6). Rather than being limited to single-layer adsorption, the latter that can be used to express heterogeneous chemical adsorption and reversible adsorption [63]is represented by Eq. (7).

$$\frac{C_e}{Q_e} = \frac{C_e}{Q_m} + \frac{1}{K_L Q_m} \quad (6)$$

$$\log Q_e = \frac{1}{n}\log C_e + \log K_F \quad (7)$$

Among them, C_e and Q_e separately denote to the Mn (VII) concentration (mg L^{-1}) and the adsorption capacity (mg g^{-1}) as adsorption equilibrium is reached; Q_m (mg g^{-1}) is the maximum amount of Mn (VII) per unit mass of the adsorbent surface; K_L and K_F stand for binding energy constants, reflecting the affinity of the adsorbent to Mn (VII); n is the Freundlich constant.

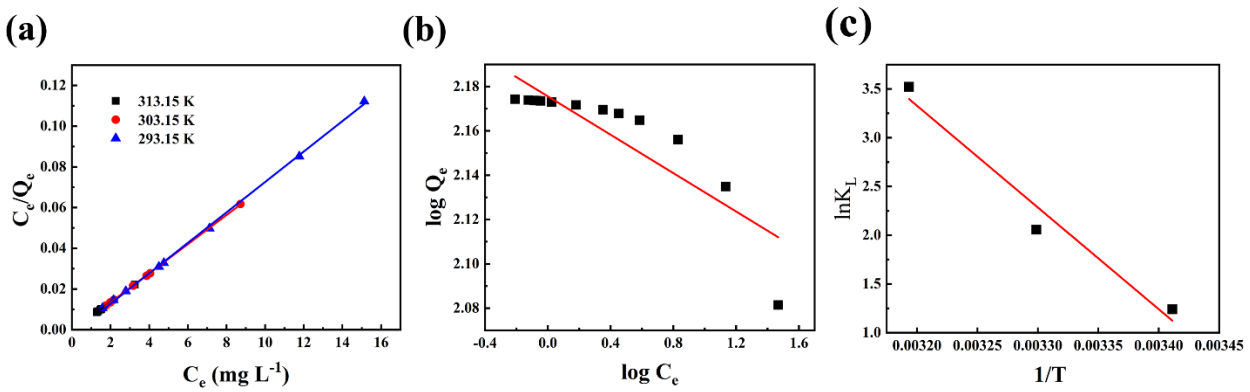

Figure 8 Langmuir isotherm model (a), Freundlich isotherm model (b) and adsorption thermodynamics (c) of Fe_3O_4@PpPD-SA adsorption of Mn (VII).

Table 2 Isotherm parameters of Fe_3O_4@PpPD-SA composite for Mn (VII) adsorption under pH=2.

	T (K)	K_L (L mg^{-1})	K_F (mg g^{-1}) (mg L-1)$^{-1/n}$	Q_m (mg g^{-1})	n	R^2	R_L
	293.15	3.46	--	133.69	--	0.99	1.93×10^{-3}
Langmuir	303.15	7.82	--	139.66	--	0.99	8.53×10^{-4}
	313.15	33.83	--	145.35	--	0.99	1.97×10^{-4}
Freundlich	--	--	149.83	--	23.08	0.76	--

Two models and the corresponding parameters of Mn (VII) adsorption by Fe_3O_4@PpPD-SA composite are shown in Figure 8 (a) (b) and Table 2. It can be easily found that Langmuir isotherm

model obtain an excellent linear fitting curve at different temperatures, while Freundlich isotherm model is not linear, which indicates that the adsorption process follows Langmuir adsorption model. Besides, from the parameters of the two models, it can be concluded that all R^2 values at various temperatures of the first model is greater than 0.99, and even at 313.15 K, the value is 0.99999. The R^2 of the second model is only 0.76271. Accordingly, Langmuir adsorption model is more aligned with the adsorption process of Mn (VII).

$$R_L = \frac{1}{K_L C_0} \tag{8}$$

Usually Eq. (8) [64]is used to calculate R_L, which is used to define the pros and cons of the adsorption process. If $R_L>1$, adsorption will be hindered; if $R_L=1$, it is linear adsorption; if $0<R_L<1$, it is beneficial to the adsorption. In here, all R_L values of 1.93×10^{-3}, 8.53×10^{-4} and 1.97×10^{-4} at different temperatures are less than 1. Hence, Fe_3O_4@PpPD-SA composite favors to adsorb Mn (VII).

On the basis of the above analyses, pseudo second-order model displays that the adsorption process is linear with the concentrations of adsorbent and adsorbed ion concurrently. Intra-particle diffusion model demonstrates that the third stage (micropore diffusion) and the fourth stage (equilibrium stage) are the main steps for controlling the adsorption process. Langmuir adsorption model indicates that the adsorption process is monolayer adsorption. The combination of these model results fully describe the adsorption process of Fe_3O_4@PpPD-SA adsorption for Mn (VII).

3.2.4 Adsorption thermodynamics

Eq. (9) and Eq. (10) are used to research the thermodynamic parameter of Fe_3O_4@PpPD-SA composite for Mn (VII) adsorption.

$$\Delta G = -RT \ln K_L \tag{9}$$

$$\ln K_L = \frac{\Delta S}{R} - \frac{\Delta H}{RT} \tag{10}$$

In which R is the universal gas constant（J mol^{-1} K^{-1}); ΔS is the entropy change (J mol^{-1} K^{-1}).

Table 3 Adsorption thermodynamic parameters of Fe_3O_4@PpPD-SA composite for Mn (VII) adsorption under pH=2.

T (K)	ΔG (kJ mol^{-1})	ΔS (J mol^{-1} K^{-1})	ΔH (kJ mol^{-1})
293.15	-3.03		
303.15	-5.18	305.13	86.71
313.15	-9.17		

Adsorption thermodynamics diagram of lnK_L vs. 1/T is shown in Figure 8 (c). On the basis of Eq. (9), Eq. (10) and Table 2, the calculated thermodynamic data are presented in Table 3. As the adsorption temperature increases from 293.15K to 313.15K, the maximum Q values are 133.69 mg g^{-1}, 139.66 mg g^{-1}, and 145.35 mg g^{-1}, respectively. And the ΔG values are -3.03 kJ mol^{-1}, -5.18 kJ mol^{-1} and -9.17 kJ mol^{-1}, respectively. With the increase of temperature, the increased Q proves that the temperature rise is favorable for the adsorption process. The simultaneously decreased ΔG demonstrates the spontaneous adsorption process. In the light of the fitted lnK_L vs. 1/T diagram, the intercept and the slope of the line are successively used to estimate ΔH and ΔS, and their value are separately 86.71 kJ mol^{-1} and 305.13 J mol^{-1} K^{-1}. In brief, ΔG is negative, and ΔH and ΔS are positive, meaning that the adsorption process is a spontaneous endothermic reaction, as well as the randomness of the solid-liquid interface increases.

3.2.5 Adsorption cycle and selective adsorption

0.1 M H_2SO_4 is used to soak the adsorbed Fe_3O_4@PpPD-SA to remove MnO_2 from the reaction[65]. Each adsorption-desorption cycle is as a cycle, and the data obtained is shown in Figure 9 (a). Although the adsorption time increases with increasing the cycle numbers, the final adsorption of Mn (VII) by Fe_3O_4@PpPD-SA composite still maintains a high q, and only loses less than 1%

after four cycles. In the fifth cycle, the q drops by nearly 10%. This is because too many adsorption times causes insufficient binding sites on the surface of the adsorbent, making it impossible to bind Mn (VII)[66]. But in general, Fe_3O_4@PpPD-SA composite can be recycled as a heavy metal ion adsorbent and has a good development prospect.

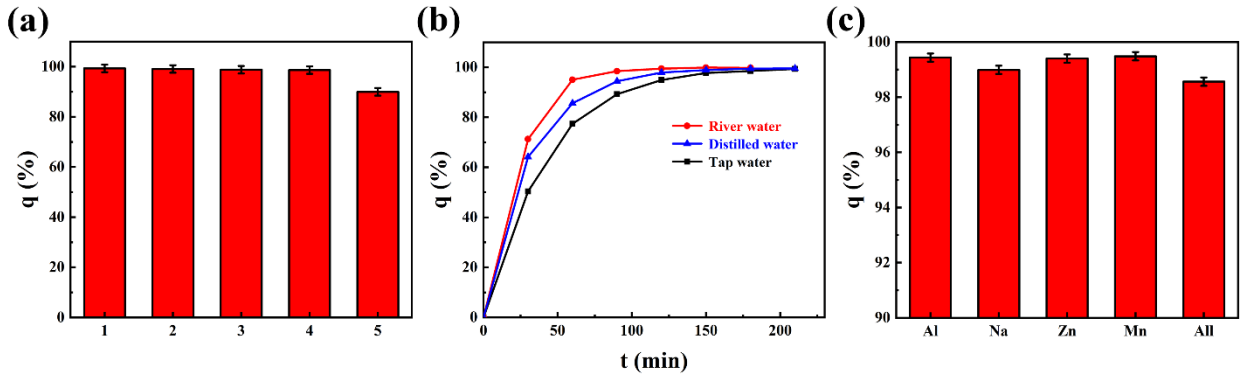

Figure 9 Cyclic adsorption of Fe_3O_4@PpPD-SA composite for Mn (VII) (a), the q in different water samples (b) and the effect of different metal ions on the q (c).

Figure 9 (b) describes the adsorption effect of Fe_3O_4@PpPD-SA composite on Mn (VII) in three different kinds of water samples including river water, tap water and distilled water. It can be clearly seen that the adsorption is most effective in river water. This may be attributed to the presence of microorganisms in the river water playing a certain role, and it also shows that Fe_3O_4@PpPD-SA composite can be well used in the purification of actual sewage. The adsorption effect of tap water is worse than that of distilled water, which may be ascribed to the fact that the tap water itself contains many ions. These ions are competitive in the process of Fe_3O_4@PpPD-SA composite adsorbing Mn (VII). Hence, the inferior adsorption performance is presented for tap water.

Figure 9 (c) depicts the impact of other ions on the adsorption of Mn (VII) by Fe_3O_4@PpPD-SA composite. Adding equal proportions of Al^{3+}, Na^{+} and Zn^{2+} ions into the Mn (VII) solution, the q of Fe_3O_4@PpPD-SA composite on Mn (VII) is slightly reduced, with a loss of less than 0.5%. In the adsorption experiment of a solution with all the above ions, the loss of q is nearly 1%. Although the introduced ions will compete with Mn (VII) for the adsorption sites on Fe_3O_4@PpPD-SA composite, leading to the reduction of the q, the prepared composite still shows very strong q to Mn

(VII).

4 Conclusion

In here, a high-efficiency adsorbent of Fe_3O_4@PpPD-SA composite was designed and fabricated for removing Mn (VII). The influences of adsorption time, temperature and pH are researched elaborately. The results show that the q increases with the increase of temperature. In the case of pH=2, the Q can reach up to 148.34 mg g^{-1}. The adsorption mechanism of Fe_3O_4@PpPD-SA composite is ascribed to the synergy effect of coordination complex and electrostatic adsorption. Furthermore, the investigation of the adsorption kinetics and thermodynamics show that the adsorption conforms to pseudo-second order adsorption kinetics model and Langmuir adsorption isotherm model. The rate-controlling steps of the reaction are mainly determined by the third stage (Micropore diffusion) and the fourth stage (Equilibrium stage) of intraparticle diffusion. The negative ΔG, the positive ΔH and ΔS indicate that the adsorption process is a spontaneous endothermic process. In addition, after four adsorption cycle tests, the adsorption capacity losses only 1%, exhibiting a good cycle utilization rate. Fe_3O_4@PpPD-SA composite for Mn (VII) has high q in river water and mixed metal ions solution and exhibits practical application value.

Acknowledgement

We gratefully appreciate the support of the Natural Science Foundation of Shandong (ZR2019BB063). The author gratitude the environmental and function material team, supported by the Project of Shandong Province Higher Educational Young Innovative Talent Introduction and Cultivation. The authors would like to thank Zhu Dejing from Shiyanjia Lab (www.shiyanjia.com) for the BET analysis. The authors gratefully acknowledge financial support from Taif University Researchers Supporting Project number (TURSP-2020/32), Taif University, Taif, Saudi Arabia.

Conflict of Interest

The authors declare that they have no conflict of interest.

References

[1] Sun, Z., Zhang, Y., Guo, S., Shi, J., Shi, C., Qu, K., Qi, H., Huang, Z., Murugadoss, V., Huang, M., Guo, Z.: FConfining FeNi nanoparticles in biomass-derived carbon for effectively photo-Fenton catalytic reaction for polluted water treatment. Adv. Compos. Hybrid Mater. **5**, 1566-1581 (2011)

[2] Luan, L., Tang, B., Liu, Y., Wang, A., Zhang, B., Xu, W., Niu, Y.: Selective capture of Hg(II) and Ag(I) from water by sulfur-functionalized polyamidoamine dendrimer/magnetic Fe_3O_4 hybrid materials. Sep. Purif. Technol. **257** (2021)

[3] Fu, T. T., Niu, Y. Z., Zhou, Y. Z., Wang, K., Mu, Q. H., Qu, R. J., Chen, H., Yuan, B. Q., Yang, H. W.: Adsorption of Mn(II) from aqueous solution by silica-gel supported polyamidoamine dendrimers: Experimental and DFT study. J. Taiwan Inst. Chem. Eng. **97**, 189-199 (2019)

[4] Wang, W., Ma, Y., Zhuang, Z., Zhou, S., Ma, M., Wu, Q., Bai, R., Li, T.: Synthesis of walnut-like polyaniline by using polyvinyl alcohol micellar template with excellent film transmission. J. Appl. Polym. Sci. **138**, e50701 (2021)

[5] Guo, S., Li, C., Zhang, Y., Wang, Y., Li, B., Yang, M., Zhang, X., Liu, G.: Experimental evaluation of the lubrication performance of mixtures of castor oil with other vegetable oils in MQL grinding of nickel-based alloy. J. Clean. Prod. **140**, 1060-1076 (2017)

[6] Nan, J., Guo, S., Alhashmialameer, D., He, Q., Meng, Y., Ge, R., El-Bahy S., Naik, N., Murugadoss, V., Huang, M., Xu, B., Shao, Q., Guo, Z.: Hydrothermal Microwave Synthesis of Co_3O_4/In_2O_3 Nanostructures for Photoelectrocatalytic Reduction of Cr(VI) ACS Appl. Nano Mater. **5**, 8755-8766 (2022)

[7] Wu, Q., Gao, L., Huang, M., Mersal, G., Ibrahim, M., El-Bahy, Z., Shi, X., Jiang, Q.: Aminated lignin by ultrasonic method with enhanced arsenic (V) adsorption from polluted water. Adv. Compos. Hybrid Mater. **5**, 1044-1053 (2022)

[8] Si, Y., Li, J., Cui, B., Tang, D., Yang, L., Murugadoss, V., Maganti, S., Huang, M., Guo, Z.: Janus phenol–formaldehyde resin and periodic mesoporous organic silica nanoadsorbent for the removal of heavy metal ions and organic dyes from polluted water. Adv. Compos. Hybrid Mater. **5**, 1180-1195 (2022)

[9] Deng, Z., Sun, S., Li, H., Pan, D., Patil, R., Guo, Z., Seok, Ilwoo.: Modification of coconut shell-based activated carbon and purification of wastewater. Adv. Compos. Hybrid Mater. **4**, 65-73 (2021)

[10] Wang, Y., Xie, W., Liu, H., Gu, H.: Hyperelastic magnetic reduced graphene oxide three-dimensional framework with superb oil and organic solvent adsorption capability. Adv. Compos. Hybrid Mater. **3**, 473-484 (2020)

[11] Guo, L., Zhang, Y., Zheng, J., Shang, L., Shi, Y., Wu, Q., Liu, X., Wang, Y., Shi, L., Shao, Q.: Synthesis and characterization of ZnNiCr-layered double hydroxides with high adsorption activities for Cr(VI). Adv. Compos. Hybrid Mater. **4**, 819-829 (2021)

[12] Wang, S., Yuang, N., Dai, T., Chang, Z., Liang, Y., Liu, X., Chen, Q., Hu, B., Wang, N.: Surface post-functionalization of COFs by economical strategy via multiple-component one-pot tandem reactions and their application in adsorption of pesticides. Adv. Compos. Hybrid Mater. **5**, 1439-1449 (2022)

[13] Elayappan, V., Murugadoss, V., Fei, Z., Dyson, P. J., Angaiah, S.: Influence of polypyrrole incorporated electrospun poly(vinylidene fluoride-co-hexafluoropropylene) nanofibrous composite membrane electrolyte on the photovoltaic performance of dye sensitized solar cell. Eng. Sci **10**, 78-84 (2020)

[14] Li, G., Wang, L., Lei, X., Peng, Z., Wan, T., Maganti, S., Huang, M., Murugadoss, V., Seok, I., Jiang, Q., Cui, D., Alhadhrami, A., Ibrahim, M., Wei, H.: Flexible, yet robust polyaniline coated foamed polylactic acid composite electrodes for high-performance supercapacitors. Adv. Compos. Hybrid Mater. **5**, 853-863 (2022)

[15] Guo, J., Chen, Z., El-Bahy, Z., Liu, H., Abo-Dief, H., Abdul, W., Abualnaja, K., Alanazi, A., Zhang, P., Huang, M., Hu, G., Zhu, J.: Tunable negative dielectric properties of magnetic $CoFe_2O_4$/graphite-polypyrrole metacomposites. Adv. Compos. Hybrid Mater. **5**, 899-906 (2022)

[16] Quyang, L., Huang, W., Huang, M., Qiu, B.: Polyaniline improves granulation and stability of aerobic granular sludge. Adv. Compos. Hybrid Mater. **5**, 1126-1136 (2022)

[17] Rehman, S., Ahmed, R., Ma, K., Xu, S., Tao, T., Aslam, M., Amir, M., Wang, J.: Composite of strip-shaped ZIF-67 with polypyrrole: a conductive polymer-MOF electrode system for stable and high specific capacitance. Eng. Sci. **13**, 71-78 (2021)

[18] Wei, Y., Luo, W., Zhuang, Z., Dai, B., Ding, J., Li, T., Ma, M., Yin, X., Ma, Y.: Fabrication of ternary MXene/MnO_2/polyaniline nanostructure with good electrochemical performances. Adv. Compos. Hybrid Mater. **4**, 1082-1091 (2021)

[19] Zhuang, Z., Wang, W., Wei, Y., Li, T., Ma, M., Ma, Y.: Preparation of polyaniline nanorods/manganese dioxide nanoflowers core/shell nanostructure and investigation of electrochemical performances. Adv. Compos. Hybrid Mater. **4**, 938-945 (2021)

[20] Xie, W., Yao, F., Gu, H., Du, A., Lei, Q., Naik, N., Guo, Z.: Magnetoresistive and piezoresistive polyaniline nanoarrays in-situ polymerized surrounding magnetic graphene aerogel. Adv. Compos. Hybrid Mater. **5**, 1003-1016 (2022)

[21] Ma, Y., Ma, M., Yin, X., Shao, Q., Lu, N., Feng, Y., Lu, Y., Wujcik, E. K., Mai, X., Wang, C., Guo, Z.: Effective removal of proteins and polysaccharides from biotreated wastewater by polyaniline composites. Adv. Compos. Hybrid Mater. **in press,** https://doi.org/10.1007/s42114-022-00508-0 (2022)

[22] Wang, W., Zheng, M., Ren, J., Ma, M., Yin, X., Li, T., Ma, Y.: Fabrication of magnetic $Fe_3O_4/MnO_2/TiO_2$/polypyrrole heterostructure for efficient adsorption of Mn7+ from aqueous solution. J. Appl. Polym. Sci. **139**, e52199 (2022)

[23] Zheng, M., Wei, Y., Ren, J., Dai, B., luo, W., Ma, M., Li, T., Ma, Y.: 2-aminopyridine functionalized magnetic core–shell Fe3O4@polypyrrole composite for removal of Mn (VII) from aqueous solution by double-layer adsorption. Sep. Purif. Technol. **277**, 119455 (2021)

[24] Ismail, M. I., Azizan, N. H., Ashaari, M. M.: Isolation and Screening of Biosurfactant-Producing Marine Bacteria from Kuantan Port, Pahang, Malaysia. Herit. Sci. **2**, 21-26 (2018)

[25] Tang, X., Tang, P., Si, S., Liu, L.: Adsorption and removal of bisphenol A from aqueous solution by p-phenylenediamine-modified magnetic graphene oxide. J. Serb. Chem. Soc. **82**, 39-50 (2017)

[26] Tang, P., Si, S., Liu, L., Tang, X.: p-Phenylenediamine Functionalized Magnetic Graphene Oxide for the Removal of Congo Red from Wastewater. Nanosci. Nanotech. Lett. **8**, 148-155 (2016)

[27] Min, Y.-L., Wang, T., Zhang, Y.-G., Chen, Y.-C.: The synthesis of poly(p-phenylenediamine) microstructures without oxidant and their effective adsorption of lead ions. J. Mater. Chem. **21**, 6683-6689 (2011)

[28] Chouksey, A., Agrawal, M.: Impact of COVID-19 Pandemic on Psychological Health of College Students in India. Eng. Sci. **15**, 177-186 (2021)

[29] Dar, U. A., Salunke-Gawali, S., Shinde, D., Bhand, S., Satpute, S.: Thermal and Spectral Studies of Transition Metal Complexes of 2-Bromo-3-Hydroxynaphthalene-1,4-Dione: Evaluation of Antibacterial Activity Against Six Bacterial Strains. Eng. Sci. **15**, 105-115 (2021)

[30] Mdlalose, L., Balogun, M., Klavins, M., Deeks, C., Treacy, J., Chimuka, L., Chetty, A.: The chemistry of Cr(VI) adsorption on to poly(p-phenylenediamine) adsorbent. Water Sci. Technol. **78**, 2481-2488 (2018)

[31] Liu, Q., Liu, Q., Ruan, Z., Chang, X., Yao, J.: Removal of Cu(II) from aqueous solution using synthetic poly (catechol-diethylenetriamine-p-phenylenediamine) particles. Ecotox. Environ. Safe. **129**, 273-281 (2016)

[32] Fleming, E., Luo, Y.: Dietary Patterns During National Lockdowns are at Odds with Recommendations for Preventing Morbidity and Mortality of COVID-19. ES Food & Agroforest. **4**, 5-8 (2021)

[33] Patil, S. N., Prasad, S. R.: An Impact of Nationwide Lockdown on Physico- chemical Parameters of Bhogavati River Water. ES Energy Environ. **11**, 28-39, (2020)

[34] Li, B., Li, C., Zhang, Y., Wang, Y., Jia, D., Yang, M.: Grinding temperature and energy ratio coefficient in MQL grinding of high-temperature nickel-base alloy by using different vegetable oils as base oil. Chinese J. Aeronaut. **29**, 1084-1095 (2016)

[35] Munzhelele, E. P., Ayinde, W. B., Mudzielwana, R., Gitari, W. M.: Synthesis of Fe Doped Poly p-Phenylenediamine Composite: Co-Adsorption Application on Toxic Metal Ions (F^- and As^{3+}) and Microbial Disinfection in Aqueous Solution. Toxics **9**, 23 (2021)

[36] Min, Y. L., Wang, T., Zhang, Y. G., Chen, Y. C.: The synthesis of poly(p-phenylenediamine) microstructures without oxidant and their effective adsorption of lead ions. J. Mater. Chem. **21**, 6683-6689 (2011)

[37] Hussain, M. S., Musharraf, S. G., Bhanger, M. I., Malik, M. I.: Salicylaldehyde derivative of nano-chitosan as an efficient adsorbent for lead(II), copper(II), and cadmium(II) ions. Internat. J Biol. Macromol. **147**, 643-652 (2020)

[38] Niu, Y., Qu, R., Chen, H., Mu, L., Liu, X., Wang, T., Zhang, Y., Sun, C.: Synthesis of silica gel supported salicylaldehyde modified PAMAM dendrimers for the effective removal of Hg(II) from aqueous solution. J. Hazard. Mater. **278**, 267-278 (2014)

[39] Ahamad, T., Naushad, M., Mousa, R. H., Alshehri, S. M.: Fabrication of starch-salicylaldehyde based polymer nanocomposite (PNC) for the removal of pollutants from contaminated water. Internat. J Biol. Macromol. **165**, 2731-2738 (2020)

[40] Amoyaw, P. A., Williams, M., Bu, X. R.: The fast removal of low concentration of cadmium(II) from aqueous media by chelating polymers with salicylaldehyde units. J. Hazard. Mater. **170**, 22-26 (2009)

[41] Zhang, Y., Wu, G., Yang, Y., Sun, J., Zhang, D.: Preparation of SBA-15 mesoporous silica grafted with bis-salicylaldehyde Schiff base for uptake of Pb(II) and Cu(II) from water. J. Sol-Gel Sci. Technol. **98**, 170-182 (2021)

[42] Ramalingam, S., Subramania, A.: Effective Removal of Nitrates From the Drinking Water By Chemical and Electrochemical Methods. Eng. Sci. 15, 80-88, (2021)

[43] Zhang, Y. Y., Wu, G. H., Yang, Y., Sun, J. Y., Zhang, D. G.: Preparation of SBA-15 mesoporous silica grafted with bis-salicylaldehyde Schiff base for uptake of Pb(II) and Cu(II) from water. J. Sol-Gel Sci. Technol. **98**, 170-182 (2021)

[44] Bradl, H. B.: Adsorption of heavy metal ions on soils and soils constituents. J. colloid interf. Sci. **277**, 1-18 (2004)

[45] Mishra, S. P.: Adsorption-desorption of heavy metal ions. Curr. Sci. **107**, 601-612 (2014)

[46] Joshi, N. C., Gairola, S. P., Gururani, P.: Characterisations and adsorption behaviour of biologically synthesised Fe3O4 based hybrid nanosorbent (Fe_3O_4-BHN). Mater. Chem. Phys. **270** (2021)

[47] Sadegh, H., Ali, G. A. M., Makhlouf, A. S. H., Chong, K. F., Alharbi, N. S., Agarwal, S., Gupta, V. K.: MWCNTs-Fe_3O_4 nanocomposite for Hg(II) high adsorption efficiency. J. Mol. Liq. **258**, 345-353 (2018)

[48] Luo, W., Ma, Y., Li, T., Thabet, H. K., Hou, C., Ibrahim, M. M., El-Bahy, S. M., Xu, B. B., Guo, Z.: Overview of MXene/conducting polymer composites for supercapacitors. J. Energy Storage **52**, 105008 (2022)

[49] Akbari-Jonoush, Z., Naseri, S., Farzadkia, M., Mohajerani, H.-R., Shirzad-Siboni, M., Yang, J.-K.: Application of C-14/SiO_2-Fe_3O_4 and AC-Fe_3O_4 nanocomposite for U(VI) removal. Desalin. Water Treat. **57**, 22519-22532 (2016)

[50] Minisy, I. M., Zasonska, B. A., Petrovsky, E., Veverka, P., Sedenkova, I., Hromadkova, J., Bober, P.: Poly(p-phenylenediamine)/maghemite composite as highly effective adsorbent for anionic dye removal. React. Funct. Polym. **146** 104436 (2020)

[51] Zhang, Y., Cao, X., Wu, G., Wang, J., Zhang, T.: Quaternized salicylaldehyde Schiff base modified mesoporous silica for efficiently sensing Cu(II) ions and their removal from aqueous solution. Appl. Surf. Sci. **527**, 146803 (2020)

[52] Chen, Z., Geng, Z., Zhang, Z., Ren, L., Tao, T., Yang, R., Guo, Z.: Synthesis of Magnetic Fe_3O_4@C Nanoparticles Modified with -SO_3H and -COOH Groups for Fast Removal of Pb^{2+}, Hg^{2+}, and Cd^{2+} Ions. Eur. J. Inorg. Chem. **2014**, 3172-3177 (2014)

[53] Lin, Z., Pan, Z., Zhao, Y., Qian, L., Shen, J., Xia, K., Guo, Y., Qu, Z.: Removal of $Hg(^{2+})$ with Polypyrrole-Functionalized Fe_3O_4/Kaolin: Synthesis, Performance and Optimization with Response Surface Methodology. Nanomaterials-Basel **10**, 1370 (2020)

[54] Polishchuk, D., Nedelko, N., Solopan, S., Slawska-Waniewska, A., Zamorskyi, V., Tovstolytkin, A., Belous, A.: Profound Interfacial Effects in $CoFe_2O_4/Fe_3O_4$ and $Fe_3O_4/CoFe_2O_4$ Core/Shell Nanoparticles. Nanoscale Res. Lett. **13** (2018)

[55] Pitzschel, K., Bachmann, J., Montero-Moreno, J. M., Escrig, J., Goerlitz, D., Nielsch, K.: Reversal modes and magnetostatic interactions in $Fe_3O_4/ZrO_2/Fe_3O_4$ multilayer nanotubes. Nanotechnology **23**, 495718 (2012)

[56] Zhang, Z., Niu, Y., Chen, H., Yang, Z., Bai, L., Xue, Z., Yang, H.: Feasible One-Pot Sequential Synthesis of Aminopyridine Functionalized Magnetic Fe_3O_4 Hybrids for Robust Capture of Aqueous Hg(II) and Ag(I). ACS Sustain. Chem. Eng. **7**, 7324-7337 (2019)

[57] Panczuk-Figura, I., Kolodynska, D.: Biodegradable chelating agent for heavy metal ions removal. Sep. Sci. Technol. **51**, 2576-2585 (2016)

[58] Turhan, O., Ors, D.: Grafted silica gel for removal of heavy metal ions. Fresen. Environ. Bull. **29**, 7706-7724 (2020)

[59] Kong, C., Zhao, X., Li, Y., Yang, S., Chen, Y. M., Yang, Z.: Ion-Induced Synthesis of Alginate Fibroid Hydrogel for Heavy Metal Ions Removal. Front. Chem. **7**, 905 (2020)

[60] Yin, R. T., Niu, Y. Z., Zhang, B. S., Chen, H., Yang, Z. L., Yang, L. X., Cu, Y. M.: Removal of Cr(III) from aqueous solution by silica-gel/PAMAM dendrimer hybrid materials. Environmen. Sci. Pollut. R. **26**, 18098-18112 (2019)

[61] Shen, Y., Jiang, N., Liu, S., Zheng, C., Wang, X., Huang, T., Guo, Y., Bai, R.: Thiol functionalization of short channel SBA-15 through a safe, mild and facile method and application for the removal of mercury (II). J. Environ. Chem. Eng. **6**, 5420-5433 (2018)

[62] Sezgin, N., Balkaya, N.: Removal of heavy metal ions from electroplating wastewater. Desalin. Water Treat. **93**, 257-266 (2017)

[63] Jia, J., Wu, A., Luan, S.: Spectrometry recognition of polyethyleneimine towards heavy metal ions. Colloid. Surface. A **449**, 1-7 (2014)

[64] Kong, N., Huang, X., Cui, L., Liu, J.: Surface Modified Graphene for Heavy Metal Ions Adsorption. Sci. Adv. Mater. **5**, 1083-1089 (2013)

[65] Lei, Z., Yao, Y., Yusu, W., Lei, Z., Yang, J., Yuzhen, H.: Study on denitration performance of MnO_2@CeO_2 core-shell catalyst supported on nickel foam. Appl. Phys. A **128** (2022)

[66] Sun, C. W., Xie, Y., Ren, X. M., Song, G., Alsaedi, A., Hayat, T., Chen, C. L.: Efficient removal of Cd(II) by core-shell Fe_3O_4@polydopamine microspheres from aqueous solution. J. Mol. Liq. **295**, 10 (2019)